Eur. Phys. J. A **13**, 33–37 (2002)

THE EUROPEAN PHYSICAL JOURNAL A

Low-lying states of ^{6}He studied via the ^{6}Li(t, ^{3}He)^{6}He reaction

T. Nakamura[a]

Department of Physics, Tokyo Institute of Technology, 2-12-1 Oh-okayama, Meguro, Tokyo 152-8551, Japan

Received: 1 May 2001 / Revised version: 31 August 2001

Abstract. We present the recent experimental results on the ^{6}He structure studied by the ^{6}Li(t, ^{3}He)^{6}He reaction at 336 MeV. Above the conspicuous peaks for ground and first excited states for ^{6}He, we have observed a broad structures at $E_x \sim 5$ MeV, and $E_x \sim 15$ MeV. The angular distribution of this structure exhibits the dominance of a $\Delta L = 1$ transition, indicating the existence of intruder dipole states at low excitation energies in ^{6}He. A slight admixture of positive-parity states in this structure has been indicated as well.

PACS. 25.60.Lg Charge-exchange reactions – 21.10.Pc Single-particle levels and strength functions – 27.20.+n $6 \leq A \leq 19$

1 Introduction

Neutron halos and skins offer an opportunity to study the wealth of phenomena associated with the closeness of the particle threshold. In particular, low-lying excited states in the continuum of these nuclei have been one of the main issues in nuclear halo/skin physics. Transition strength in the continuum may reflect the twofold structure composed of a core and a surrounding cloud of very diffuse valence neutron(s). In the Coulomb dissociation of halo nuclei, for example, a substantially large $E1$ concentration at low excitation energies has been observed [1–6]. This excitation has now been well understood as a large direct-breakup cross-section due to a spatially extended halo state, rather than as the excitation to collective soft dipole resonance.

A further interesting structure in the continuum of loosely bound nuclei may be related to the "Borromean" structure as in ^{6}He. A Borromean nucleus is a three-body quantum bound system where any of its two-body subsystems is unbound. In this case the excitation of a low-lying continuum structure, such as a three-body 2^+ resonance, has been predicted by three-body theories [7–10].

As for the discrete states of halo/skin nuclei, the low-lying intruder states play an important role. For instance, the one-neutron halo nucleus ^{11}Be contains an intruder $2s_{1/2}$ neutron configuration in its ground state where the $1p_{1/2}$ configuration is normally expected. The low-energy dipole excitation at $E_x \sim 1.3$ MeV was observed for ^{11}Li, indicating that the ground and/or excited states contain strong intruder configurations [11,12].

Here we have studied the low-lying structure of ^{6}He by means of the charge-exchange reaction ^{6}Li(t, ^{3}He)^{6}He. Since in the case of ^{6}He reliable information on the core-n interaction exists, this nucleus serves as a prototype for understanding the Borromean continuum structure. ^{6}He is unique in that its core ^{4}He is a very hard spherical nucleus and its proton shell is closed. This is in contrast with the structure of other halo nuclei where intruder states are often caused by deformation in the core or strong p-n residual interactions as in the ^{11}Be case [13–15]. In spite of these interests, the level structure of ^{6}He has not been well understood except for the ground state ($J^\pi = 0^+$) and the first excited state ($E_x = 1.8$ MeV, $J^\pi = 2^+$) [16]. Hence, the detailed study for the ^{6}He structure has been called for.

2 The (t, ^{3}He) reaction as a spectroscopic tool

The (n, p)-type charge-exchange reaction on ^{6}Li at intermediate energy is one of the useful tools to approach the structure of ^{6}He since simple distorted-wave theory is applicable. The important point of this reaction is that one can determine the orbital angular momentum of each state in the residual nucleus since the angular distribution of the ejectile is strongly correlated with the orbital angular momentum transfer $\Delta\boldsymbol{L}$. Indeed $\Delta\boldsymbol{L}$ can be described simply by $\Delta\boldsymbol{L} = \boldsymbol{q} \times \boldsymbol{R} = \boldsymbol{k} \times \theta\boldsymbol{R}$, where $\boldsymbol{q}$, $\boldsymbol{k}$, θ, $\boldsymbol{R}$ denote momentum transfer, incident momentum, scattering angle, and the mean reaction radius, respectively. With this consideration, for example, the forward-peaked angular distribution in the Gamow-Teller transition ($\Delta\boldsymbol{L} = 0$) can be readily understood.

The (n, p) reaction is the simplest of this type among charge-exchange reactions. However, since the neutron

[a] e-mail: nakamura@ap.titech.ac.jp

beam is secondary, the (n,p) reaction suffers from low statistics and poor energy resolution, of the order of 1 MeV. Hence, it appears to be difficult to resolve even the first excited state from the ground state of ^{6}He in the ^{6}Li$(n,p)^6$He reaction [17,18].

Recently, the $(^7\mathrm{Li},^7\mathrm{Be})$ reaction as an alternative to (n,p) was used [19–21] for a ^{6}Li target, where a low-lying structure at $E_\mathrm{x} \sim 5$ MeV in ^{6}He was observed. However, there was some disagreement about the nature of this structure. References [19,21] claimed that this structure occurs as a dipole excitation, while ref. [20] assigned this structure to be a 2^+ state. One difficulty in using this reaction arises from the complicated reaction mechanism associated with the heavy-ion projectile ^{7}Li. In particular, the spin-parity assignment from the angular distribution is rather ambiguous, due to the fact that this reaction is accompanied by $\boldsymbol{\Delta L}$ both for the projectile and the target, namely, $\boldsymbol{\Delta L} = \boldsymbol{\Delta L}(^7\mathrm{Li} \rightarrow {}^7\mathrm{Be}) + \boldsymbol{\Delta L}(^6\mathrm{Li} \rightarrow {}^6\mathrm{He})$. Here $\boldsymbol{\Delta L}(^7\mathrm{Li} \rightarrow {}^7\mathrm{Be}) = 0$ or 2. Hence, the angular distribution is obtained by many combinations of projectile and target angular momentum transfers [20]. It should be noted that the angular distribution for (n,p) is characterized by an orbital momentum transfer only for a target transition, namely $\boldsymbol{\Delta L} = \boldsymbol{\Delta L}(^6\mathrm{Li} \rightarrow {}^6\mathrm{He})$, since there is no orbital angular momenta in n and p.

The $(\mathrm{t},{}^3\mathrm{He})$ reaction may become a powerful spectroscopic tool and possibly provide a better alternative to the (n,p) and $(^7\mathrm{Li},^7\mathrm{Be})$ reactions. For this reaction, however, one has to overcome the fact that most accelerator facilities do not permit to accelerate triton beams as a primary beam for the sake of radiation safety. At the National Superconducting Cyclotron Laboratory (NSCL), Michigan State University, the triton beam has been successfully developed as a secondary beam produced by the intermediate-energy fragmentation reaction [22,23]. Using a dispersion matching technique, one can reach an energy resolution of a few hundred keV even though the secondary triton beam has a large momentum spread. The use of the S800 spectrograph with its wide angular acceptance ($\Delta\Omega = 20$ msr) enables us to obtain angular distribution with only a few angular settings, which compensates for the low intensity of the secondary beam.

Furthermore, the reaction mechanism of $(\mathrm{t},{}^3\mathrm{He})$ is analogous to (n,p), which facilitates the analysis of the reaction. For example, only $\Delta L = 0$ is allowed for a projectile transition, the same as for (n,p), so that the angular distribution is only sensitive to the orbital angular momentum transfer for the target, *i.e.* $\boldsymbol{\Delta L}(^6\mathrm{Li} \rightarrow {}^6\mathrm{He})$. It is also important to note that similarities are seen between the (p,n) and the $({}^3\mathrm{He},\mathrm{t})$ reactions [24], the latter being mirror reaction of $(\mathrm{t},{}^3\mathrm{He})$.

3 Experiment

The experiment was performed by using the S800 spectrograph at the NSCL. The triton beam delivered as a secondary beam had a typical intensity of about 10^6 particles/s, a mean energy of 336 MeV with an energy spread of 1%. It was used to bombard a ^{6}Li target with a thickness of 17.4 mg/cm^2 (95% enriched). The ^{7}Li contaminants in the target hardly affect the spectrum. This is because up to $E_\mathrm{x} = 7.7$ MeV in ^{6}He there is no contribution from the $^7\mathrm{Li}(\mathrm{t},{}^3\mathrm{He})^7\mathrm{He}$ reaction due to the different reaction Q value. For higher excitations no significant contribution from ^{7}Li is expected due to the small structureless charge-exchange strengths as shown in the $^7\mathrm{Li}(n,p)^7\mathrm{He}$ experiment [18].

The momentum of the outgoing ^{3}He ions was measured by the spectrograph operated in dispersion matching mode. Data were taken at three different angular settings centered at 0, 8 and 18 degrees. These settings covered the laboratory scattering angle, θ_lab, of about 0–5, 4–12, and 14–22 degrees, respectively. The more detailed description of the experimental setup is given in ref. [25].

4 Experimental results

Figure 1 shows the energy spectra obtained for the $^6\mathrm{Li}(\mathrm{t},{}^3\mathrm{He})^6\mathrm{He}$ reaction at the 0°(a) and 8°(b) settings of the S800. Besides the conspicuous peaks for the transitions to the ground and first excited states in ^{6}He, the spectra show strong and broad structures at $E_\mathrm{x} \sim 5$ MeV and ~ 15 MeV. The structure around 15 MeV is notable at the higher angular setting, while the amplitude for the 5 MeV structure rapidly decreases as θ_lab increases. An interesting feature of the 5 MeV bump is its very asymmetric shape.

The spectral shape from the 0 degree setting (fig. 1(a)) was analyzed by Gaussian peak-fitting. The asymmetric structure around 5 MeV was decomposed into three Gaussians to better study the nature of its components. This division is arbitrary, although at least three Gaussians are necessary to obtain an overall agreement of this structure, indicating its complex composition. The best fit values for the locations of three Gaussians were 4.4 ± 0.1 MeV, 7.7 ± 0.2 MeV and 9.9 ± 0.4 MeV, respectively. The structure around 15 MeV was best fitted by a single Gaussian with a centroid of 14.6 ± 0.2 MeV, consistent with the results from the (n,p) [18] and $(^7\mathrm{Li},^7\mathrm{Be})$ reactions [20]. The continuum background (dotted curves in fig. 1) is estimated with a semi-phenomenological parameterization of the quasi-free scattering, *i.e.* the $p_\mathrm{bound}(\mathrm{t},{}^3\mathrm{He})n$ reaction [20].

Differential cross-sections as a function of momentum transfer q are shown in fig. 2 for the ground and the first excited states, and in fig. 3 for the higher excited states. These angular distributions have a strong dependence on the orbital angular momentum transfer ΔL. Distorted Wave Born Approximation (DWBA) calculations were performed with the computer code DW81 [26]. Optical-model parameters of a Woods-Saxon shape were extracted from our elastic scattering measurement of ^{3}He on ^{6}Li at 335 MeV at the 8 degree setting of the S800. The effective projectile-nucleon (t-N) interactions were based on the effective ^{3}He-N interactions derived phenomenologically for the $({}^3\mathrm{He},\mathrm{t})$ reaction with various targets by Van der Werf *et al.* [27,28].

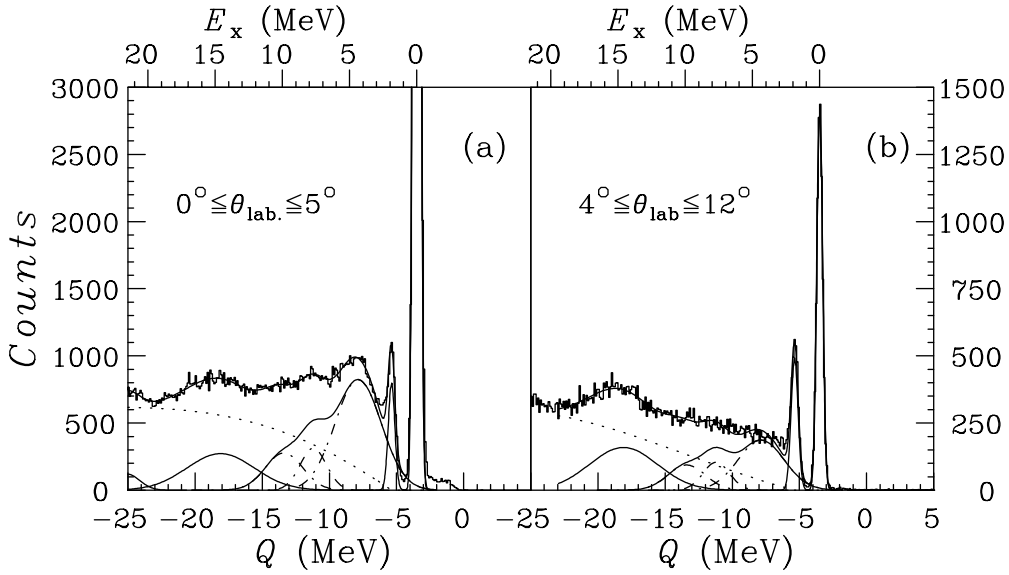

Fig. 1. Energy spectra for the ^{6}Li(t, ^{3}He)^{6}He reaction measured at 336 MeV for (a) 0 degree setting of the S800 (0°–5°), and (b) 8 degree setting (4°–12°).

The wave functions and one-body transition densities for the input for DW81 were calculated with the shell-model computer code OXBASH [29]. Here we assumed harmonic-oscillator (HO) radial wave functions. The positive-parity states were calculated in the $1p$ shell basis with the CKHE interaction [30,31], which reflects the influence of the special neutron halo/skin nature of the neutron-rich He isotopes. For the negative-parity states we use the *s-p-sd-pf* model space with the WBT interaction of Warburton and Brown [32]. The configurations assumed for these negative-parity states involve the excitation of one nucleon from the $1s$ shell to the $1p$ shell or one nucleon from the $1p$ shell to the $1d2s$ shell. The detail of the ^{6}He energy levels calculated from these shell-model are discussed elsewhere [25].

Comparisons of the DWBA calculation with the experimental angular distributions for the ground and the first excited states are shown in fig. 2. The transition to the ground state (^{6}Li(1^+)→ ^{6}He(0^+)) has a forward-peaked distribution, typical of a Gamow-Teller transition, while the transition to the first excited state (^{6}Li(1^+)→ ^{6}He(2^+)) has a much broader shape, indicating a large mixture of a $\Delta L = 2$ transition. The distribution for the ground state transition is in good agreement with the DWBA calculation (solid curve), in particular for the forward angles up to $q \sim 1.5$ fm^{-1}. The normalization factor here is 1.0. For the first excited state, reasonable agreement of the data with the DWBA calculation is obtained. The shape is characterized by a mixture of $\Delta J = 0$ (mostly $\Delta L = 0$) and $\Delta J = 2, 3$ transitions (mostly $\Delta L = 2$), as expected. The normalization factor for the calculated distribution is 0.8.

The angular distributions for the 5 MeV and 14.6 MeV structures are shown in fig. 3(a) and fig. 3(b), respectively. As described above, the 5 MeV bump was decomposed into three Gaussians that peak at 4.4 MeV, 7.7 MeV and

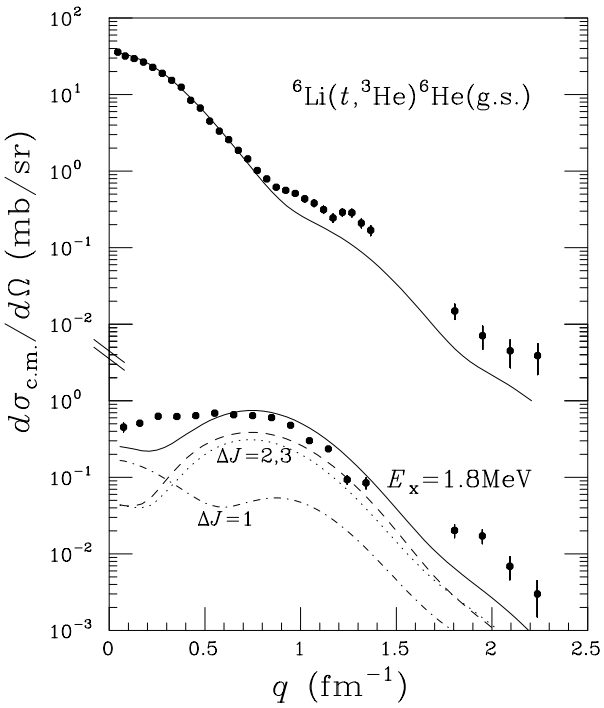

Fig. 2. Differential cross-sections for the ground and first excited states of ^{6}He. Solid curves show the results of DWBA calculations. The calculated $\Delta J = 1, 2$, and 3 components for the first excited state are shown as dot-dashed, dotted, and dashed curves, respectively.

9.9 MeV. These angular distributions are clearly broader than that of the ground state with $\Delta L = 0$, and narrower than that of the first excited state with $\Delta L = 2$ dominant. This fact suggests that the transition to the 5 MeV structure has $\Delta L = 1$ characteristics, indicating the existence of low-lying dipole states in ^{6}He. On the other

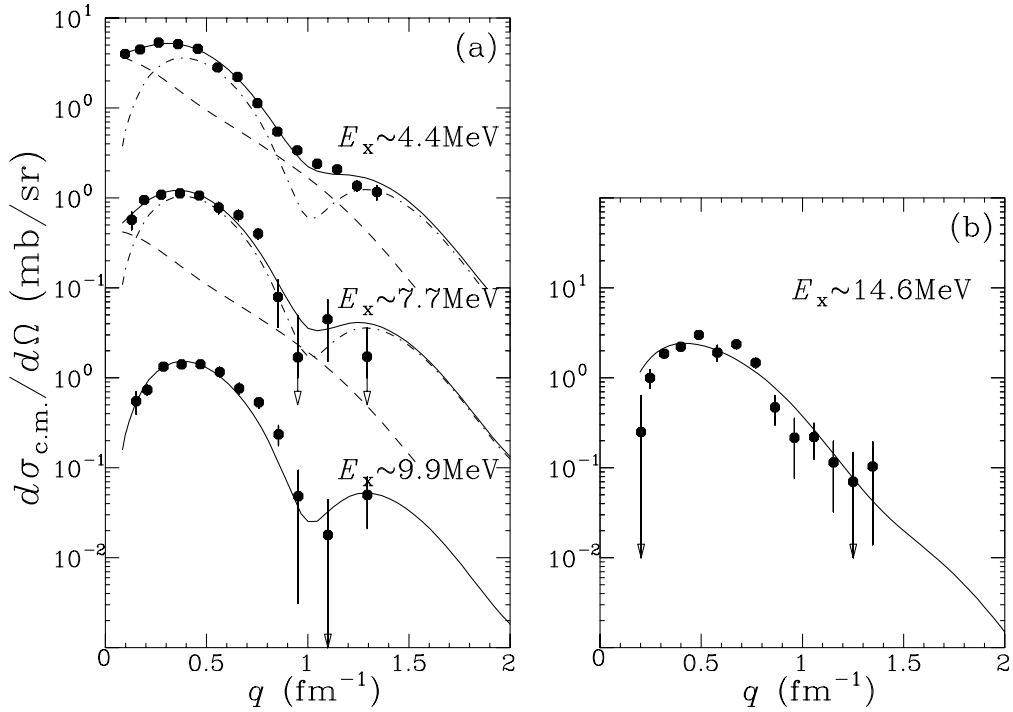

Fig. 3. Differential cross-sections for the 5 MeV structure (a), and 14.6 MeV structure (b). Solid curves show the results of DWBA calculations. For the 5 MeV structure (a), The contributions from the negative- and positive-parity states are shown by the dot-dashed and dashed curves, respectively.

hand, the cross-section at $q \sim 0$ for the 4.4 MeV region is larger than for the 7.7 MeV and 9.9 MeV regions, suggesting that the structure has a small $\Delta L = 0$ component at the lower excitation energies, mixed with the $\Delta L = 1$ component. Indeed, the DWBA calculation shows that the best agreement is obtained with an admixture of transitions to negative-parity states ($\Delta L = 1$), with those to the positive-parity states ($\Delta L = 0, 2$) being only at lower excitation energies.

The angular distribution for the 14.6 MeV structure is shown in fig. 3(b). The distribution is broader than those for the 5 MeV structure. The distribution is well reproduced assuming that the transition occurs to the predicted negative-parity states at $E_x \sim$ 16–20 MeV [25]. In fig. 3(b) the calculation for the 1_3^- state is shown by the solid curve, which is in good agreement with the data.

The difference between the $\Delta L = 1$ transition to the 5 MeV and 14.6 MeV structures is that the former is dominated by a transition to $2s1p^{-1}$(proton hole in the $1p$ orbital and neutron in $2s$ orbital in ^{6}Li), while the latter is dominated by the transition to $1p1s^{-1}$ and $1d1p^{-1}$ configurations. By considering that the simple relation $\boldsymbol{\Delta L} = \boldsymbol{q} \times \boldsymbol{R} = 1\hbar$ for dipole transitions, the difference of angular distributions is naturally understood by that of matter distributions between $1s$ and $2s$ orbitals. Since the $2s$ orbital has a larger mean radius (R) than that for the $1s$ orbital, the angular distribution (in q space) is narrower for the 5 MeV structure. The result indicates that some part of $2s$ orbitals is lowered down to about 5 MeV above the $1p$ orbital. This gap energy is significantly smaller than the energy between $1s$ and $1p$ orbitals of about 15 MeV.

5 Summary

In conclusion we have measured the ^{6}Li(t, ^{3}He)^{6}He reaction at 336 MeV. We have observed a broad asymmetric structure at $E_x \sim$ 5 MeV and another structure at 14.6 MeV, as well as strong peaks for the well-known ground and first excited states in ^{6}He. The angular distributions for these states are consistently analyzed using the DWBA calculation. The structure around 5 MeV is dominated by the negative-parity states with a small mixture of positive-parity states in its lower-energy portion. The existence of intruder states at such low energies suggests a quenching of the $1p$-$2s$ gap in this nucleus. The 14.6 MeV structure has been found to have a $\Delta L = 1$ shape, corresponding to the transition composed mainly of $1p1s^{-1}$ and $1d1p^{-1}$ components. Due to the conspicuous difference in angular distribution by the $\boldsymbol{\Delta L}$ from the target to residue, we have demonstrated that the (t, ^{3}He) reaction at the intermediate energies offers a very good spectroscopic opportunity for a neutron rich nucleus such as ^{6}He.

This work has been done in colloboration with T. Aumann, D. Bazin, Y. Blumenfeld, B.A. Brown, J. Caggiano, R. Clement, T. Glasmacher, P.A. Lofy, A. Navin, B.V. Prytychenko, B.M. Sherrill, and J. Yurkon. We acknowledge S. Van der Werf, for fruitful and invaluable discussions. This work is supported in part by the National Science Foundation under Contract Nos. PHY-9528844 and PHY-9605207.

References

1. T. Nakamura *et al.*, Phys. Lett. B **331**, 296 (1994).

2. S. Shimoura *et al.*, Phys. Lett. B **348**, 29 (1995).
3. K. Ieki *et al.*, Phys. Rev. Lett. **70**, 730 (1993); D. Sackett *et al.*, Phys. Rev. C **48**, 118 (1993).
4. M. Zinser *et al.*, Nucl. Phys. A **619**, 151 (1997).
5. T. Nakamura *et al.*, Phys. Rev. Lett. **83**, 1112 (1999).
6. T. Aumann *et al.*, Phys. Rev. C **59**, 1252 (1999).
7. S. Aoyama, S. Mukai, K. Kato, K. Ikeda, Prog. Theor. Phys. **93**, 99 (1995); S. Aoyama, S. Mukai, K. Kato, K. Ikeda, Prog. Theor. Phys. **94**, 343 (1995).
8. B.V. Danilin *et al.*, Phys. Rev. C **55**, R577 (1997); B.V. Danilin, I.J. Thompson, J.S. Vaagen, M.V. Zhukov, Nucl. Phys. A **632**, 383 (1998).
9. S.N. Ershov *et al.*, Phys. Rev. C **56**, 1483 (1997).
10. A. Cobis, D.V. Fedorov, A.S. Jensen, Phys. Rev. Lett. **79**, 2411 (1997).
11. A.A. Korsheninnikov *et al.*, Phys. Rev. Lett. **78**, 2317 (1997).
12. H. Simon *et al.*, Phys. Rev. Lett. **83**, 496 (1999).
13. I. Talmi, I. Unna, Phys. Rev. Lett. **4**, 469 (1960).
14. H. Esbensen, B.A. Brown, H. Sagawa, Phys. Rev. C **51**, 1274 (1995).
15. H. Sagawa, B.A. Brown, H. Esbensen, Phys. Lett B **309**, 1 (1993).
16. F. Ajzenberg-Selove, Nucl. Phys. A **490**, 1 (1988); D.R. Tilley *et al.*, to be published in Nucl. Phys. A (2002).
17. K. Wang *et al.*, Phys. Rev. C **38**, 2478 (1988).
18. F. Brady *et al.*, Phys. Rev. Lett **51**, 1320 (1983).
19. S.B. Sakuta *et al.*, Europhys. Lett. **22**, 511 (1993).
20. J. Jänecke *et al.*, Phys. Rev. C **54**, 1070 (1996).
21. S. Nakayama *et al.*, Phys. Rev. Lett **85**, 262 (2000).
22. I. Daito *et al.*, Phys. Lett. B **418**, 27 (1998).
23. B.M. Sherrill *et al.*, Nucl. Instrum. Methods, A **432**, 299 (1999).
24. I. Bergqvist *et al.*, Nucl. Phys. A **469**, 648 (1987).
25. T. Nakamura *et al.*, Phys. Lett. B **493**, 209 (2000).
26. R. Schaeffer, J. Raynal, DWBA70 code; extended version, J. Comfort.
27. S. Van der Werf *et al.*, Nucl. Phys. A **496**, 305 (1989).
28. S. Van der Werf, private communication.
29. B.A. Brown, A. Etchegoyen, W.D.M. Rae, N. S. Godwin, computer code OXBASH, 1984, unpublished.
30. J. Stevenson *et al.*, Phys. Rev. C **37**, 2220 (1988).
31. S. Cohen and D. Kurath, Nucl. Phys. **73**, 1 (1965).
32. E.K. Warburton, B.A. Brown, Phys. Rev. C **46**, 923 (1992).
33. D. Aleksandrov *et al.*, Nucl. Phys. A **669**, 51 (2000).